Ore Geology Reviews 139 (2021) 104545

Contents lists available at ScienceDirect

Ore Geology Reviews

journal homepage: www.elsevier.com/locate/oregeorev

Zinc isotope composition of the Proterozoic clastic-dominated McArthur River Zn-Pb-Ag deposit, northern Australia

Raphael J. Baumgartner [a,b,*], Marcus Kunzmann [a], Sam Spinks [a], Xiaopeng Bian [c], Seth G. John [c], Teagan N. Blaikie [a], Siyu Hu [a]

[a] CSIRO Mineral Resources, Australian Resources Research Centre, Kensington, WA, Australia
[b] School of Biological, Earth and Environmental Sciences, The University of New South Wales, Kensington, NSW, Australia
[c] Department of Earth Sciences, University of Southern California, Los Angeles, CA, USA

ARTICLE INFO

Keywords:
Clastic-dominated zinc-lead deposits
McArthur River Zn-Pb-Ag deposit
Zinc isotopes
Ore genesis
Ore exploration

ABSTRACT

This study provides a Zn isotope characterization (δ^{66}Zn) of the c. 1,640 Ma clastic-dominated McArthur River Zn-Pb-Ag deposit. Dolomitic, siltstone-hosted sulfide ores were sampled in two separate drill cores. One intersects the stratiform, vertically stacked orebodies at the centre of the deposit, and the other one intersects the south-eastern periphery of the deposit. The analyzed ores show relatively invariable δ^{66}Zn values typical of the continental crust (0.35 ‰ median with 0.05 ‰ standard deviation). This signature is consistent with (near-) quantitative sulfide (sphalerite) precipitation during ore formation, negligible Zn isotope fractionation during fluid transport, and perhaps muted fractionation associated with near-quantitative Zn extraction from the source. Hence, our data show that a pronounced Zn isotope fractionation pattern characterized by lower δ^{66}Zn values closer to the hydrothermal source, as reported from other Zn-Pb deposits, is not developed within the McArthur River deposit. However, across some orebodies, we note a subtle Zn isotope fractionation trend that correlates with the relative abundances of several temperature-sensitive base and trace metals (Zn, Pb, and Ag). This trend can be explained by subtle influence of Rayleigh-type Zn isotope fractionation during fluid evolution and Zn sulfide precipitation. Previous studies have suggested that Zn isotopes may be useful in the exploration for economic mineralization, as these studies observed both a significant Zn isotope halo and δ^{66}Zn values markedly different from the continental crust. However, because both characteristics are not observable at McArthur River, the Zn isotope system may not have been useful in finding this deposit.

1. Introduction

Previous Zn isotope studies of major Zn-Pb sulfide deposits, including the Irish-type Zn-Pb deposits (Wilkinson et al., 2005), the Zn-Pb deposits in the Red Dog district (Kelley et al., 2009), and the Alexandrika volcanic-hosted massive sulfide deposit (Mason et al., 2005), reported a distinct and systematic Zn isotope variation in sphalerite that is marked by increasing δ^{66}Zn values with increasing distance to the hydrothermal source. This variation was interpreted as being the result of kinetic (Rayleigh-type) Zn isotope fractionation during fluid cooling and Zn-sulfide precipitation (Wilkinson et al., 2005, in press; Mason et al., 2005; Kelley et al., 2009). Fluid mixing may exhibit an additional control on Zn isotope composition, whereas isotopic fractionation associated with Zn speciation and redox reactions (cf. Kavner et al., 2008; Moynier et al., 2017) was considered negligible. Although the Zn isotope characteristics of other Zn deposits and prospects were studied in recent years (e.g., Gagnevin et al., 2012; Zhou et al., 2014a,b; Gao et al., 2018; Wang et al., 2018), it is still an open question if a systematic spatial Zn isotope trend is generally developed across Zn-Pb deposits, and whether ore-forming processes can account for Zn isotope signals markedly different from the continental crust. Addressing these issues by further studying major Zn-Pb sulfide deposits is important, especially to better understand if and how Zn isotopes may be applicable in the exploration for economically important mineralization.

Here, we report the first Zn isotope study of the c. 1640 Ma McArthur River (also known as Here's Your Chance; HYC) Zn-Pb-Ag deposit of the McArthur Basin in northern Australia, with an estimated pre-mining resource of 227 Mt at 9.2% Zn, 4.1% Pb, 41 g/t Ag, and 0.2% Cu (Logan et al., 1990). Whole rock samples of eight vertically stacked orebodies, which consist of sphalerite-galena-pyrite-rich bands hosted

* Corresponding author at: CSIRO Mineral Resources, Australian Resources Research Centre, Kensington, WA, Australia.
E-mail address: raphael.baumgartner@csiro.au (R.J. Baumgartner).

https://doi.org/10.1016/j.oregeorev.2021.104545
Received 16 August 2021; Received in revised form 13 October 2021; Accepted 26 October 2021
Available online 30 October 2021

by pyritic and dolomitic, organic matter-rich siltstones, were sampled in two drill cores: one intersecting the centre of the deposit near the inferred fluid source, and one further away at the south-eastern fringe of the deposit. We show that the recorded Zn isotope values are typical for the continental crust and show only slight variations that may be reconciled with an influence by kinetic isotope fractionation during ore formation. The implications of these findings for ore genesis, and the use of Zn isotopes in ore exploration, are discussed.

2. Geological setting and deposit geology

2.1. Regional geology

The McArthur River deposit is located in the southern McArthur Basin (Fig. 1), which is part of a large multiphase Proterozoic basin system on the North Australia Craton (Scott et al., 2000; Giles et al., 2002; Betts et al., 2003; Betts and Giles, 2006; Selway et al., 2006; Gibson et al., 2017; Blaikie and Kunzmann, 2020). The southern McArthur Basin contains a well preserved, 5–15 km thick carbonate-siliciclastic succession with bimodal igneous rocks in the lower parts (Jackson et al., 1987; Rawlings, 1999). The McArthur River deposit is hosted by the c. 1640 Ma Barney Creek Formation within the McArthur Group (Fig. 2), a 1–3.5 km thick mixed carbonate-siliciclastic package. The deposition of the McArthur Group generally reflects thermal subsidence, yet the onset of deposition of the lower Barney Creek Formation in the middle McArthur Group coincided with roughly north–south directed extension, which resulted in a complex restructuring of the basin, including the development of kilometre- to a few tens of kilometre-scale sub-basins and paleohighs (McGoldrick et al., 2010; Blaikie and Kunzmann, 2020).

The Barney Creek Formation comprises the W-Fold Shale Member, the HYC Pyritic Shale Member, and the Cooley Dolostone Member

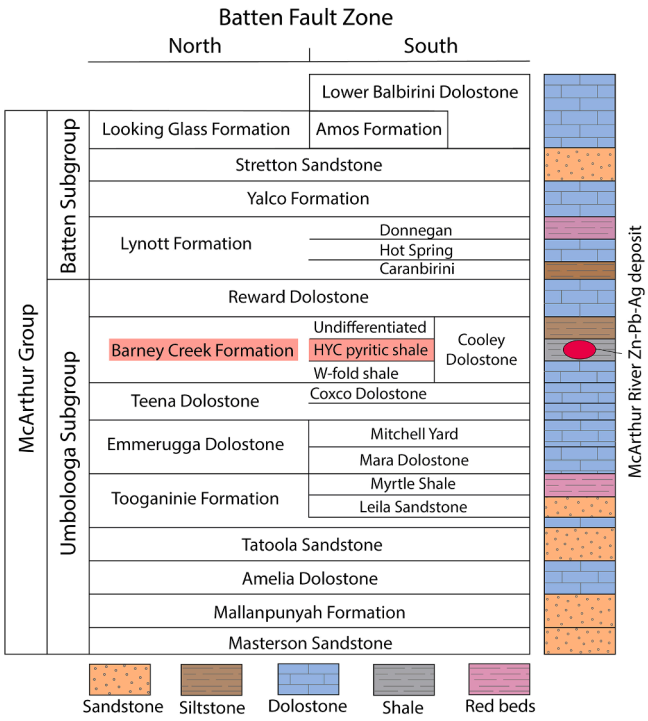

Fig. 2. Paleoproterozoic to Mesoproterozoic stratigraphy of the southern McArthur Basin, Northern Territory, Australia (redrawn after Rawlings 1999; Kunzmann et al., 2019). The stratigraphic position of the McArthur River Zn-Pb-Ag deposit is indicated. See Kunzmann et al. (2019, 2020) for facies analysis and sequence stratigraphy of the lower to middle McArthur Group.

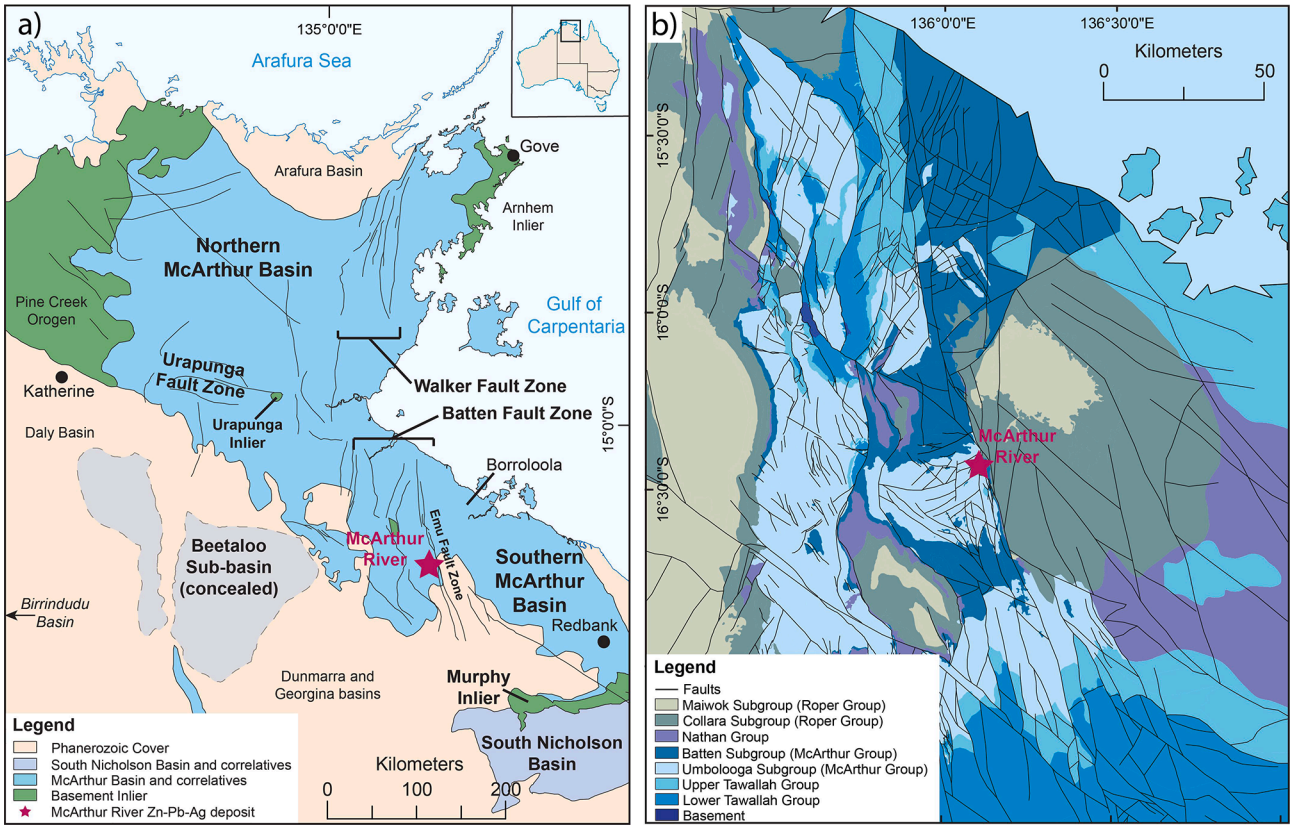

Fig. 1. Simplified geological map of the McArthur Basin (a) and interpreted solid geology map of the southern McArthur Basin (b). Modified after Blaikie and Kunzmann (2020).

(Jackson et al., 1987; Fig. 2). These members, which are overlain by the undifferentiated upper part of the formation, were defined in the HYC sub-basin, and at least partially represent lateral facies changes (Jackson et al., 1987). This is particularly important for the Cooley Dolostone, a dolostone breccia that occurs along local fault scarps, such as in the HYC sub-basin, where it interfingers with the other members of the Barney Creek Formation (Jackson et al., 1987). The W-Fold Shale, which is the basal member of the Barney Creek Formation, is represented by green to red dolomitic siltstone and pink dolomudstones (Brown et al., 1978; Jackson et al., 1987; Davidson and Dashlooty, 1993; Kunzmann et al., 2019). The HYC Pyritic Shale Member comprises organic-rich, dolomitic and pyritic siltstone and silty shale, which were deposited by turbidity currents and from hemipelagic settling in offshore and offshore transition environments (Bull, 1998; Kunzmann et al., 2019). Similarly, the upper undifferentiated part of the formation is dominated by dolomitic siltstone turbidite deposits, but also contains carbonate grain flow and debris flow deposits and silty shale (Kunzmann et al., 2019).

2.2. Deposit geology

The stratiform McArthur River Zn-Pb-Ag deposit is hosted by organic- and sulphide-rich dolomitic siltstones of the HYC Pyritic Shale Member. It is located in the 1–2 × 5 km large HYC sub-basin, which is bound to the east by the Western Fault, a splay of the crustal-scale Emu Fault System (Fig. 1). Eight vertically stacked ore bodies, which are separated by mass-flow breccias and undisturbed sedimentary strata, represent laterally extensive horizons of sphalerite- and galena-rich, variably pyritic and organic-rich, dolomitic siltstones and silty shales (Croxford, 1968; Croxford and Jephcott, 1972; Lambert, 1976; Williams et al., 1978; Large et al., 1998; Perkins and Bell, 1998; Chen et al., 2003; Ireland et al., 2004a,b; among others).

The prevalence of finely laminated base metal sulfides, and the presence of laminated ore clasts within intermittent mass-flow breccias, has long been viewed as evidence for syndepositional ore formation from an euxinic and hypersaline basinal brine; i.e., sulfide precipitated in the water column and/or during the onset of diagenesis in the uppermost sediment regime (e.g., Croxford, 1968; Croxford and Jephcott, 1972; Large et al., 1998; Ireland et al., 2004a,b). In this model, the Emu Fault System east of the ore deposit (Fig. 3) acted as a fluid conduit for hot hydrothermal fluids that recharged the basinal brines with metals (e.g., Large et al., 1998; Cooke et al., 2000).

Whereas hydrothermal sourcing from the Emu Fault System was indisputably a key factor in ore formation, other studies reported textural and geochemical evidence, as well as thermodynamic modelling, that supports a post-depositional, diagenetic-epigenetic origin of the ores. In this model, percolating hydrothermal fluids reacted with the buried, organic matter-rich, pyritic and dolomitic siltstones, which triggered base metal sulfide precipitation (Eldridge et al., 1993; Hinman, 1996; Perkins and Bell, 1998; Logan et al., 2001; Spinks et al., 2021). Textural evidence for a diagenetic-epigenetic origin of the ores includes: i) the presence of polymetallic sulfides that are interpreted as having precipitated after the latest episodes of diagenetic pyrite growth (Eldridge et al., 1993); and ii) sphalerite ± galena replacing laminated and nodular, sedimentary to diagenetic carbonate (Hinman, 1996; Spinks et al., 2021).

3. Sampling and analytical methods

3.1. Sample selection

Hand samples of the McArthur River Zn-Pb-Ag deposit were collected in 2016 from two drill cores. One drill core intersected the stratigraphically upper ore bodies (5–8) near the centre of the deposit, whereas all the ore bodies (1–8) were intersected at the south-eastern fringe of the deposit (Figs. 3 and 4). The centre deposit drill core is closest (~100 m) to the inferred hydrothermal fluid source, the Emu Fault Zone, whereas the south-eastern fringe drill core is at least c. 800 m away from the first drill core and c. 500 m from the nearest point of the Emu Fault Zone (Fig. 3a). Both drill cores were stratigraphically logged, and representative samples of ore bodies and weakly mineralized interbeds (Table S1 and Fig. 4) were selected for petrographical/mineralogical examination as well as chemical and Zn isotope analysis.

3.2. Optical microscopy and XRF elemental mapping

Both optical microscopy and XRF elemental mapping was carried out on polished thin sections using equipment installed at CSIRO Mineral Resources, Perth, Australia. Reflected light microscopy was conducted using a Zeiss Axio Imager.A2, whereas Micro X-ray fluorescence (μ-XRF) element mapping for Ca, Fe, Zn, and Pb was carried out using a Bruker M4 Tornado X-ray fluorescence mapper. This instrument, which is equipped with a rhodium target X-ray tube and a XFlash silicon drift X-ray detector, was operated using 50 kV acceleration voltage and 500nA beam current. Point spacing was 30 μm, and dwell times varied between 10 and 15 ms. Elements were identified using Kα and Kβ X-ray emission lines.

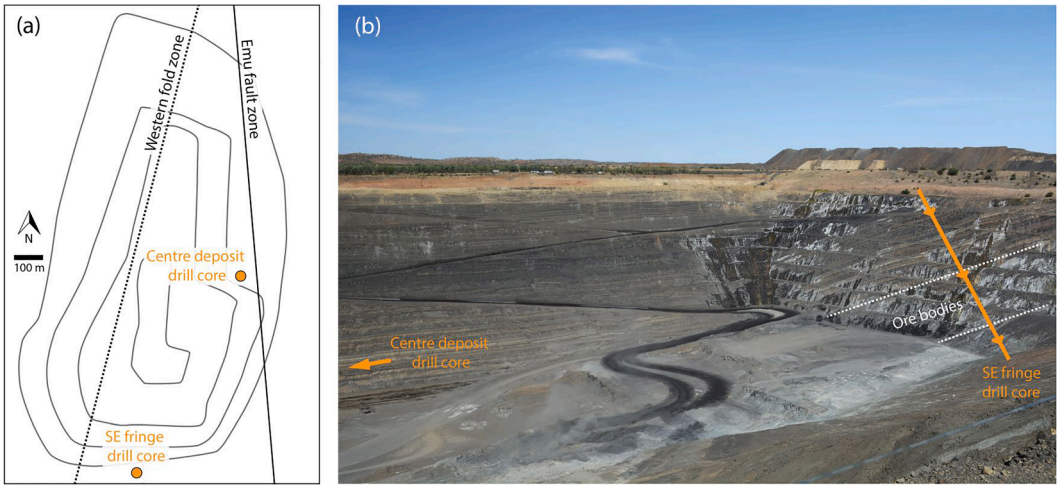

Fig. 3. Sketch map (a) and overview photograph looking southeast (b) of the McArthur River Zn-Pb-Ag open cut mine. Locations of drill cores examined in this study are indicated. Image (a) is redrawn after Spinks et al. (2020). Photograph in (b) taken with permission from McArthur River Mining Pty Ltd.

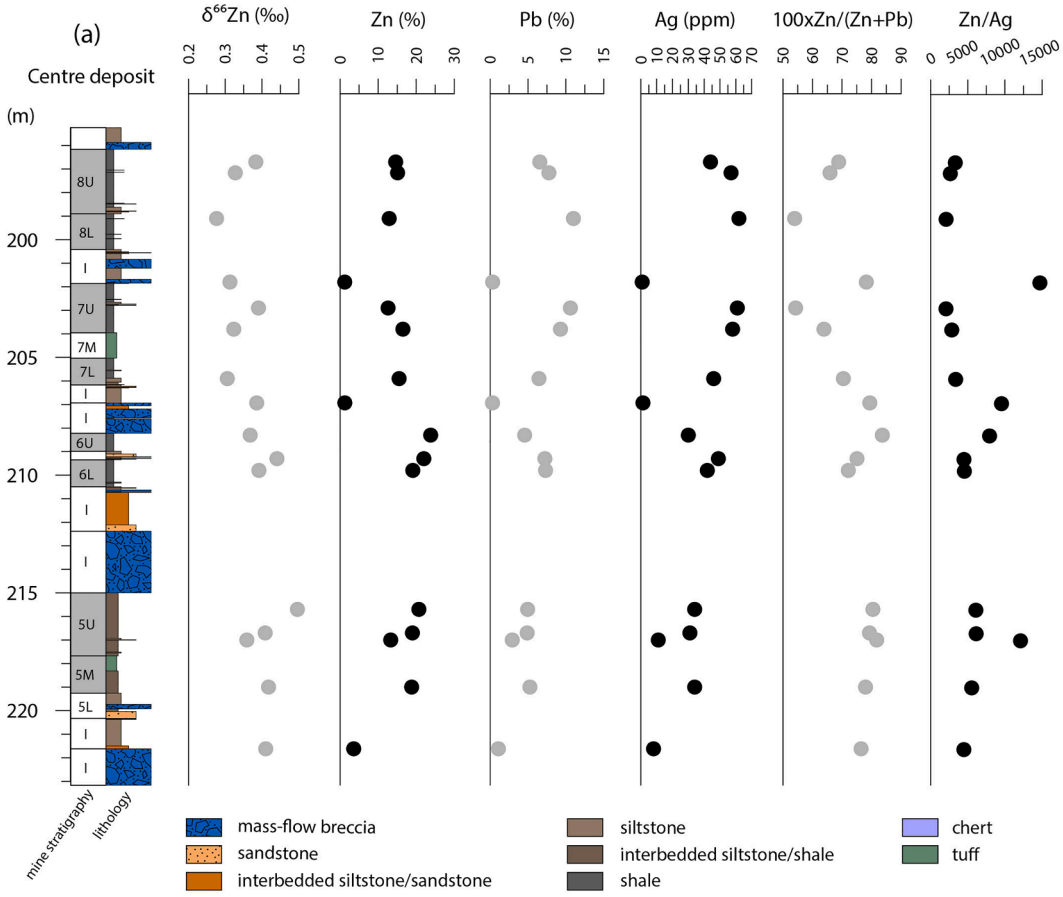

Fig. 4. Litho- and chemostratigraphic logs of drill cores intersecting the McArthur River Zn-Pb-Ag deposit at the centre (a) and the south-eastern fringe (b). See data in Table S1. Mine stratigraphy: I = Interbeds; F = footwall and ore body 1; 2–8 = ore bodies 2 to 8; L = lower; M = middle; U = upper. Whole-rock geochemical data are taken from Spinks et al. (2021).

3.3. Whole rock chemical analysis

Whole rock chemical analysis was undertaken at LabWest Minerals Analysis Pty Ltd in Perth, Australia. The samples were crushed, milled, and then microwave-digested at 160 °C and 16 bar in a mixture of hydrofluoric, nitric, phosphoric, and hydrochloric acid. Major, minor, and trace elements (i.e., Al_2O_3, CaO, FeO, K_2O, MgO, MnO, Na_2O, P_2O_5, SiO_2 and TiO_2, as well as Ag, As, Ba, Be, Cd, Ce, Co, Cr, Cs, Cu, Dy, Er, Eu, Ga, Gd, Ge, Hf, Hg, Ho, In, La, Lu, Mo, Nb, Nd, Ni, Pb, Pr, Rb, S, Sb, Sc, Se, Sm, Sn, Sr, Ta, Tb, Te, Th, Tl, Tm, U, V, W, Y, Yb, Zn and Zr) were quantified following the addition of internal standards to solutes using a combination of ICP-MS (Perkin-Elmer Nexion 300Q) and ICP-OES (Perkin-Elmer Optima 7300DV) techniques. The resulting data, which were published previously in Spinks et al. (2021), are listed together with $\delta^{66}Zn$ values in Table S1.

3.4. Zinc stable isotope analysis

Samples selected for bulk-rock Zn isotope analysis were prepared in a clean lab at the University of Southern California, USA. As most of the samples are high-grade Zn ores, and because sphalerite is the dominant host for Zn (see below), the results in this study can be directly compared with previous studies that analyzed only sphalerite (e.g., Wilkinson et al., 2005; Gagnevin et al., 2012). For each sample, an equivalent of 1.2 mg Zn was weighted into a clean 15 ml LDPE tube and doused with 15 ml of 50% HNO_3. Approximately 0.5 ml of the well-mixed suspension (~40 μg Zn) was transferred into a PFA vial, and diluted by concentrated HCl and HNO_3 following the protocol in Craddock et al. (2008) to ensure the complete digestion of sulfide and carbonate minerals. Following digestion, any precipitates were redissolved in 4 ml 10 N HCl, which resulted in a Zn concentration of c. 10 μg/mL in solution. For each sample, an aliquot containing ~ 75 ng Zn was then mixed with a ^{64}Zn-^{67}Zn double spike in amounts designed to minimize the analytical error (John et al., 2012); see Conway et al. (2013) for the isotopic composition of the spike. The sample solutions were purified by anion exchange chromatography based on established methods for $\delta^{66}Zn$ analysis (Conway et al., 2013), but 10 times greater eluent volumes were used with the addition of 250 μL AG-MP1 resin (Revels et al., 2014). Finally, the purified samples were diluted by 0.5 ml 2% HNO_3.

Zinc isotope analysis was carried out using a Neptune Multi-Collector ICPMS installed at the University of South Carolina, USA, following the procedure detailed in John et al. (2017). In short, ^{64}Zn, ^{66}Zn, ^{67}Zn and ^{68}Zn were measured, and ^{64}Ni was monitored to allow correction for potential interferences of ^{64}Ni on ^{64}Zn. A high-resolution mode was used to resolve potential polyatomic interferences of $^{40}Ar^{27}Al$ on ^{67}Zn, as well as $^{40}Ar^{28}Si$ and $^{40}Ar^{14}N^{14}N$ on ^{68}Zn. The data reduction scheme followed the iterative approach described in Siebert et al. (2001). The reported errors are the standard error based on the deviance between cycles during a single analysis (Table S1). The results are reported in delta notation with respect to the Zn isotope value of the JMC-Lyon Zn isotope standard (Maréchal et al., 1999): $\delta^{66}Zn = [(^{66}Zn/^{64}Zn)_{sample}/(^{66}Zn/^{64}Zn)_{Lyon\ JMC}-1] \times 1000$. Note here that throughout the analytical session, the NIST-682 Zn standard was used as the in-house reference material. The repeatability of the NIST-682 $\delta^{66}Zn$ value (-2.46 ‰ compared to the JMC-Lyon Zn standard; Conway et al., 2013) was better than 0.04‰ (2 SD; n = 13).

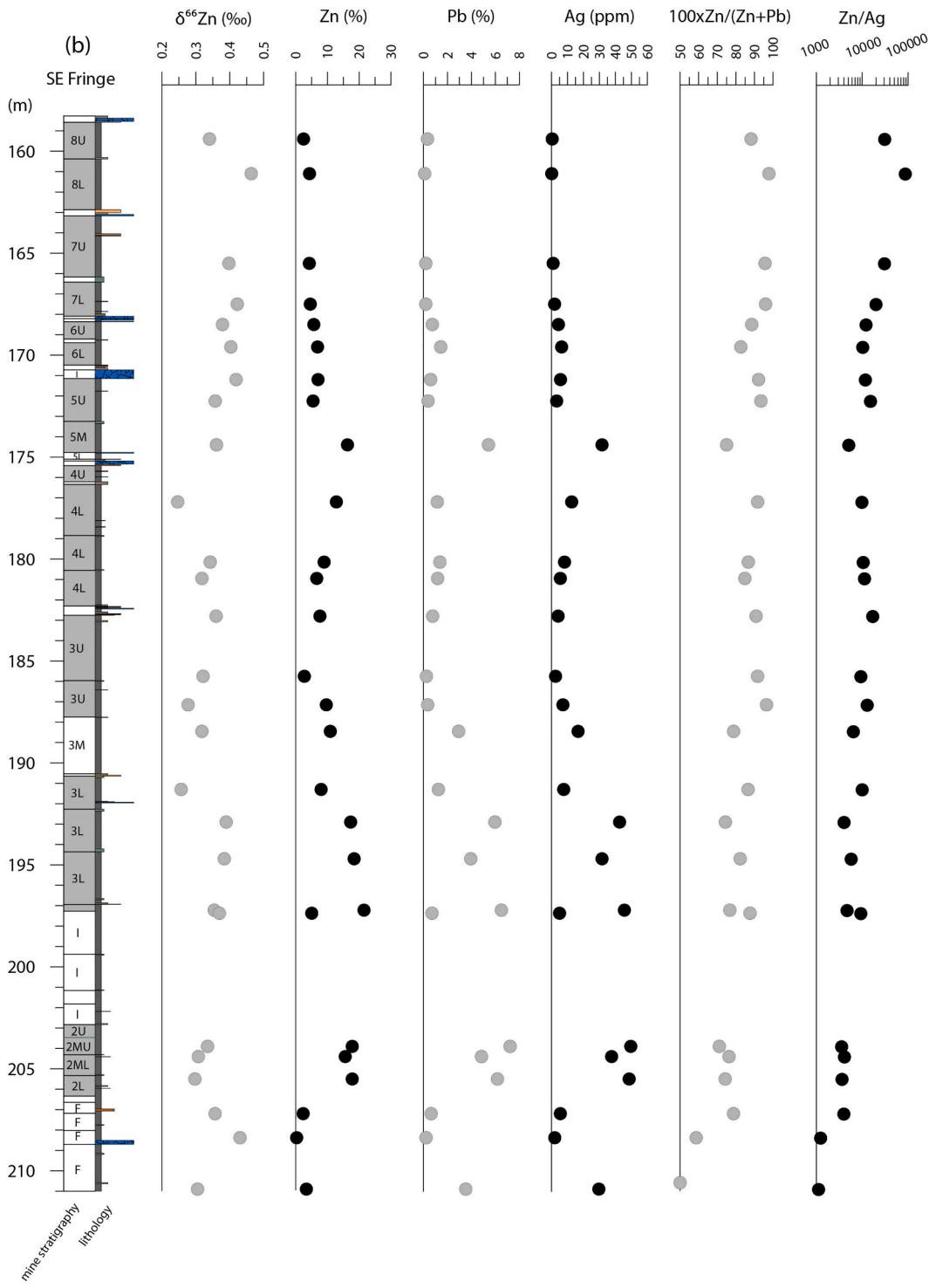

Fig. 4. (*continued*).

4. Results

4.1. Ore textures, petrography, and mineralogy

The textural, petrographic, and chemical characteristics of Zn-Pb-Ag sulfide ores from the McArthur River deposit were documented in detail in previous studies (e.g., Croxford 1968; Croxford and Jephcott, 1972; Williams, 1978; Eldridge et al., 1993; Large et al., 1998; Perkins and Bell, 1998; Ireland et al., 2004b; Dick et al., 2014; Spinks et al., 2021). Our observations are consistent with these previous studies, and therefore we only briefly summarise the features that are important for interpretation of the Zn isotope data.

Optical microscopy and high-resolution element mapping show that the layered ore sulfides, which represent up to ~ 90 vol% of the mineralized strata, are typically defined by rhythmic repetitions of thin, planar-undulating to planar-crenulated laminae that are variably disrupted by soft-sediment deformation and micro-faults (Fig. 5). These laminae comprise variable proportions of sphalerite, galena and pyrite (plus minor chalcopyrite and arsenopyrite), ranging from homogeneous laminae that are dominated by either sphalerite, galena or pyrite, to

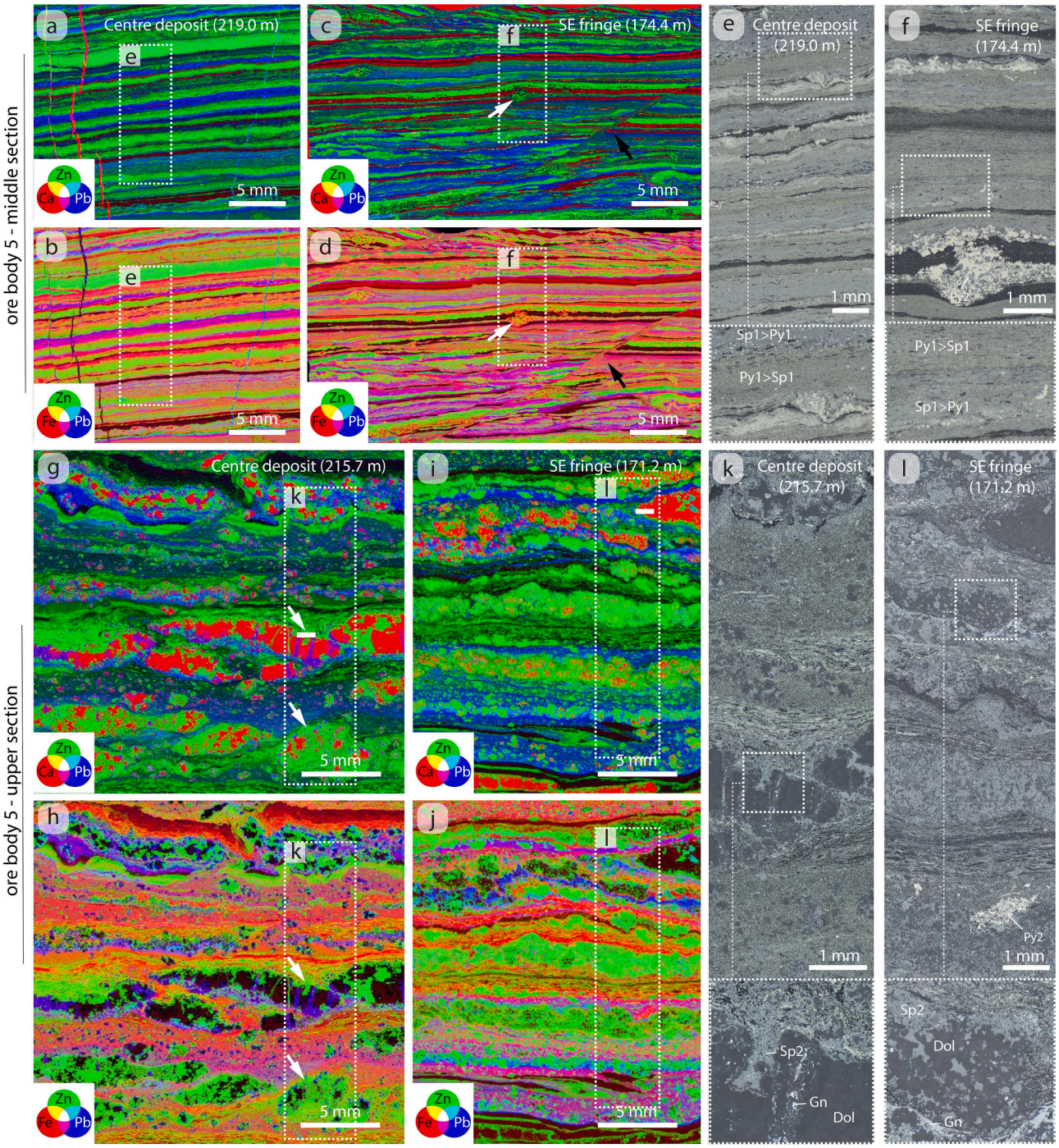

Fig. 5. Reflected light photomicrographs and element distribution maps (Ca, Fe, Zn and Pb) of thin sections of laminated sulfide ores of the McArthur River Zn-Pb-Ag deposit. Shown are representative ore textures for samples from the upper and middle sections of ore body 5 in the centre deposit and south-eastern fringe drill cores (see locations of samples in Fig. 4). Images (a-f) show rhythmic layering of essentially planar sulfide laminae containing various proportions of intimately intergrown sphalerite (Sp1), pyrite (Py1), and galena. Note within interlayered silt the presence of irregular to rounded pyrite agglomerations (Py2) that occasionally form embayments in the sulfide laminae [white arrows in (c) and (d)]. The black arrows in (c) and (d) indicate a centimetre's scale thrust within sulfide layering. Images (h-l) show wavy/crenulated, bedding-parallel sulfide layering, as well as intercalated layers of nodular and clastic dolomite [Dol; indicated by Ca in (g) and (i)] that are variably replaced by patchy sphalerite (Sp2) and lesser galena (Gn).

vertically graded intergrowths between these main sulfide phases (Fig. 5e and f). A second typical ore texture of the McArthur River deposit includes sphalerite-rich domains comprising vastly abundant carbonate; i.e., usually nodular, elongate, or irregular crystals or crystal aggregates of dolomite, which are variably overgrown and/or replaced by sphalerite as well as lesser amounts of galena and pyrite (Fig. 5g-l). Although present throughout the McArthur River Zn-Pb-Ag deposit, dolomite, and the associated sulfide replacement textures, are particularly prevalent in the SE fringe of the deposit (Ireland et al., 2004b; Spinks et al., 2021).

Micro-textural and micro-mineralogical evidence exists for several sulfide modes within the ores. The earliest pyrite (Py1, Eldridge et al., 1993; Ireland et al., 2004b) is represented by spheroidal (possibly framboidal) and euhedral grain assemblages (Fig. 5e and f). This pyrite

is intimately associated with variable proportions of fine-grained sphalerite (Sp1, Eldridge et al., 1993; Ireland et al., 2004b) and galena (Fig. 5e and f). Sphalerite that overgrows/replaces carbonate (Sp2) is more coarse-grained (up to several 100 μm) and shows a pronounced patchy habit (Fig. 5k and l; cf., Ireland et al., 2004b; Spinks et al., 2021). Lastly, minor aggregates of medium- to coarse-grained pyrite (Py2) occur within the otherwise sulfide-deficient siltstone interlayers or displace laminae that host the Py1-Sp1 assemblages (Fig. 5f and l). Previous studies reconciled the two different types of sphalerite in the ores with two competing hypotheses of ore formation: i) in syngenetic formation models, direct precipitation of Sp1 from the basinal brines, and a carbonate dissolution (replacement) origin for Sp2 during early diagenesis (e.g., Large et al., 1998); ii) in post-depositional (diagenetic-epigenetic) formation models, simultaneous precipitation of Sp1 and Sp2 from percolating hydrothermal fluids during late diagenesis (e.g., Spinks et al., 2021).

4.2. Zinc isotopes and metal abundances

Bulk-rock Zn isotope signatures (δ^{66}Zn), as well as the concentrations of Ca and selected base and trace metals (i.e., Zn, Pb, and Ag) in 42 Zn-Pb ore samples from the two examined drill cores are reported in Table S1 and illustrated in Fig. 4 and Figs. 6-9. The δ^{66}Zn values of all samples range from 0.25 to 0.50 ‰ (median 0.36 ‰ and standard deviation 0.05 ‰; Fig. 6), a spread that is larger than the analytical error of each analysis. These Zn isotope signatures are consistent with that of crustal rocks, such as mafic to felsic magmatic rocks like basalts and granites, as well as sedimentary rocks and modern deep-sea sediments (Fig. 6a). However, the median value of the McArthur River Zn isotope compositions is higher than previously reported values of both volcanic-hosted massive sulfide deposits and sediment-hosted massive sulfide deposits (Fig. 6b). The most comparable δ^{66}Zn values – though other than in this study acquired by analysing sulfide separates – were reported from the Dongshengmiao Zn-Pb-Ag deposit in China (c.f., Gao

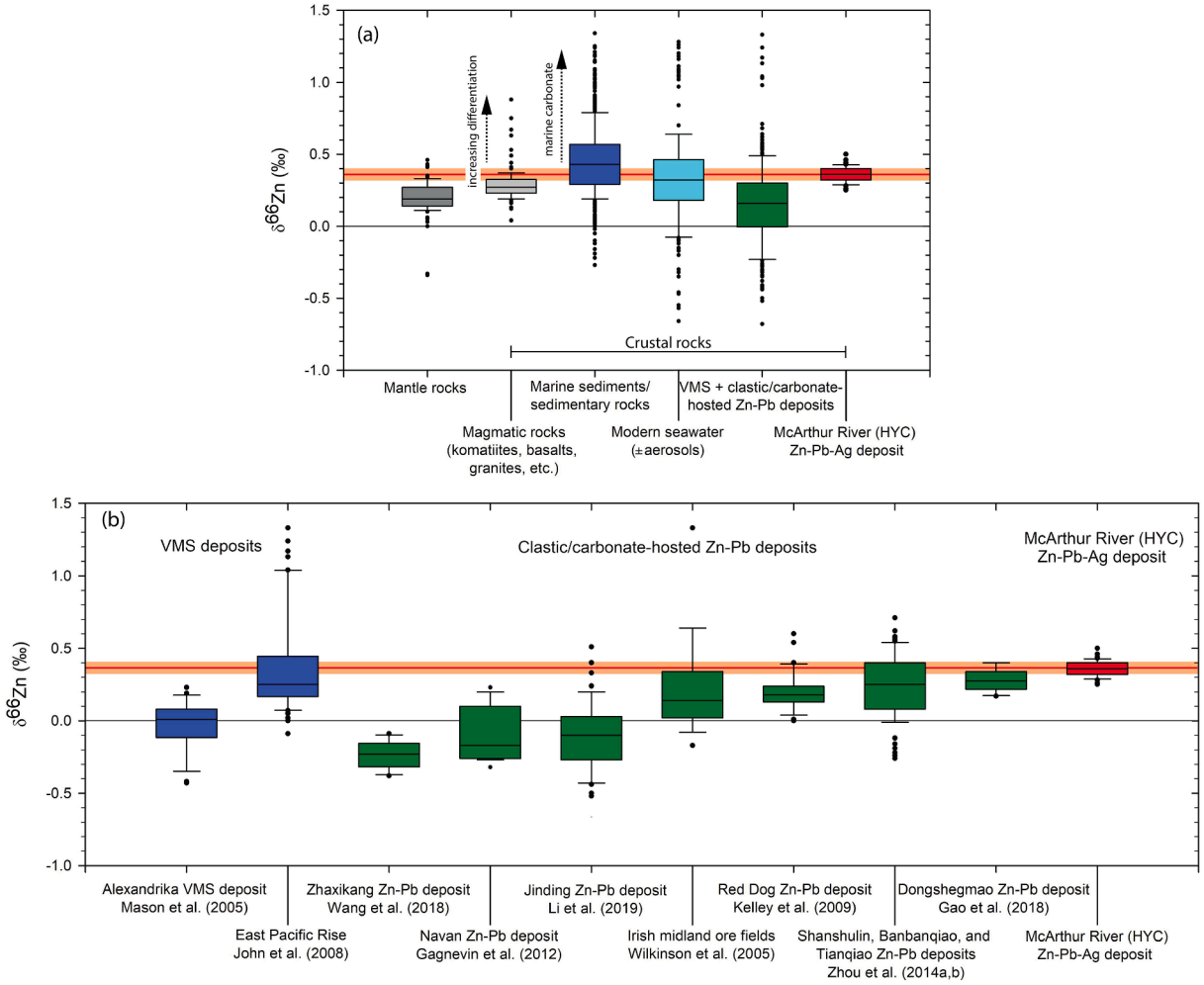

Fig. 6. Compilation of Zn isotope (δ^{66}Zn) data from different crustal reservoirs. (a) Summary of δ^{66}Zn data for mantle rocks, magmatic rocks, marine sediments and sedimentary rocks (dolostones, shales, etc.), modern seawater (±aerosols), and clastic/carbonate-hosted plus VMS polymetallic sulfide deposits. The spread of δ^{66}Zn values in magmatic rocks may in part correspond to influence by magmatic differentiation [indicated in (a)]. Marine carbonates plot on the upper end of the range in Zn isotope compositions of marine sedimentary rocks; i.e., high δ^{66}Zn values [indicated in (a)]. (b) Summary of δ^{66}Zn data of VMS deposits and clastic/carbonate-hosted polymetallic sulfide deposits. In contrast to other deposits, the McArthur River Zn-Pb-Ag ores show narrowly distributed δ^{66}Zn values within the range of the continental crust. Data sources: mantle rocks and magmatic rocks from Maréchal et al. (2000), Telus et al. (2012), Chen et al. (2013), Zhou et al. (2014a), Doucet et al. (2018), Wang et al. (2017), Sossi et al. (2018), Huang et al. (2018a,b), Xu et al. (2019); marine sediments and sedimentary rocks from Maréchal et al. (2000), Pichat et al. (2003), Bentahila et al. (2008), Kunzmann et al. (2013), Conway and John (2014), Zhou et al. (2014a,b), Little et al. (2016), Isson et al. (2017), John et al. (2017); modern seawater ± aerosols from Maréchal et al. (2000), John and Conway (2014), Little et al. (2014), Vance et al. (2016); clastic/carbonate-hosted and VMS polymetallic sulfide deposits from Wilkinson et al. (2005), John et al. (2008), Kelley et al. (2009); Mason et al. (2005), Gagnevin et al. (2012), Li et al. (2019), Zhou et al. (2014a,b), Gao et al. (2018), and Wang et al. (2018). Boxplot representation: line within box = median; box = upper and lower quartiles; whiskers = 1.5 × interquartile range, circles = outliers.

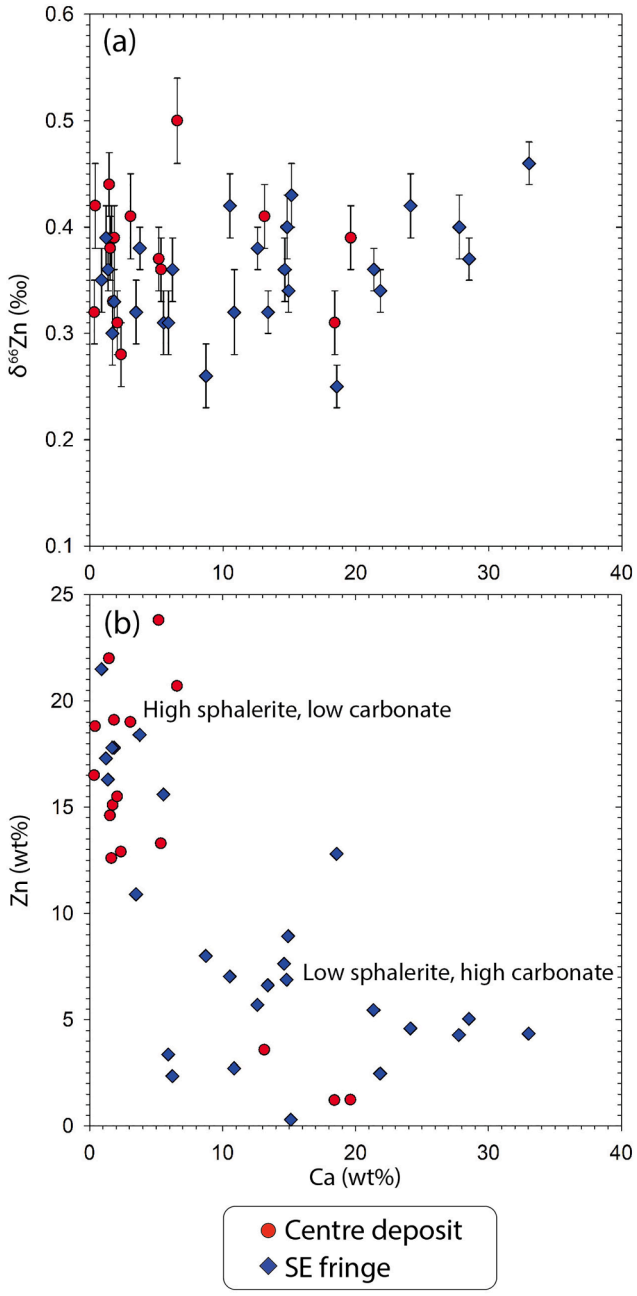

Fig. 7. Plots of (a) δ^{66}Zn versus Ca, and (b) Zn versus Ca in ore samples from the McArthur River Zn-Pb-Ag deposit. Note the lack of correlation between Ca and δ^{66}Zn. The plot in (b) indicates two trends reflecting the relative prominence of sphalerite-rich, thinly laminated ore textures (Fig. 5 a-f), and comparatively sphalerite-poor, carbonate replacement ore textures (Fig. 5g-l). The whole-rock Zn and Ca data are from Spinks et al. (2021).

et al., 2018).

Ensuring the validity of direct comparisons between the whole rock δ^{66}Zn data and previous reports of δ^{66}Zn acquired on sulfide separates requires that, for the samples studied here, sphalerite controls the δ^{66}Zn composition. Overall, no systematic relationship exists between whole rock δ^{66}Zn values and the textural, petrographic, and mineralogical characteristics of the examined ore samples. This observation is also consistent with the lack of correlation between δ^{66}Zn and carbonate content (approximated by Ca in whole-rock analysis; Fig. 7a). Importantly, the anticorrelation between Ca and Zn in the entire set of analyzed ore samples, plus the absence of a clear relationship between both elements in the subset of low sphalerite, high carbonate samples (Fig. 7b), align with the results from XRF elemental mapping in that sphalerite is the dominant host of Zn, whereas concentrations in carbonate and other sulfide phases (pyrite and galena) are deemed negligible (Fig. 5). Taken together, these observations strongly suggest that sphalerite controls the whole rock Zn concentrations and δ^{66}Zn values, and that contributions from other hosts are insignificant.

Considering all samples together, no distinctive covariation exists between δ^{66}Zn and the relative abundance of the temperature-sensitive base metals Zn and Pb [depicted as 100 × Zn/(Zn + Pb); Huston and Large, 1987]; (Fig. 8a). However, considering only the orebodies that are intersected in both drill cores (ore bodies 5–8; Fig. 4), a statistically significant, positive correlation between δ^{66}Zn and 100 × Zn/(Zn + Pb) is observed (Fig. 8b). Overall, samples from the centre of the deposit show increases in 100 × Zn/(Zn + Pb) and Zn/Ag with depth; values increase from min. 54.0 to max. 83.9 and from min. 2,066 to max. 12,091, respectively from the shallow orebodies 7 and 8 to the deeper orebodies 5 and 6 (Fig. 9a and b-c). Samples from the south-eastern fringe of the deposit show an inverse covariation; 100 × Zn/(Zn + Pb) decreases from max. 97.7 in the relatively shallow orebody 8 to min. 48.8 in the deeper orebody 1, and Zn/Ag decreases from max. 86,800 to min. 1,120 (Fig. 9c). The δ^{66}Zn values in samples from the deposit centre increase with increasing depth (i.e., from ore bodies 7 and 8 to ore bodies 5 and 6) in parallel with increasing 100 × Zn/(Zn + Pb) and Zn/Ag values, whereas the opposite relationships appear to characterize samples from the south-eastern fringe drill core (Fig. 9c and d).

5. Discussion

5.1. Zinc isotope fractionation and implications for ore genesis

Considering that nearly all Zn in the studied ore samples resides in sphalerite, the observed δ^{66}Zn values of whole rock samples cannot be explained by a significant contribution of Zn from minerals unrelated to the mineralization process, such as silicates and carbonates of the host rock. To understand the near-homogeneous and crustal Zn isotope composition of the McArthur River deposit, all the potential processes influencing Zn isotopes within this mineral system require consideration: i) leaching and extraction of metals from the source, ii) mixing of two or more (hydrothermal) fluids with contrasting Zn isotope signatures; and iii) equilibrium and/or kinetic (Rayleigh) isotope fractionation during fluid evolution and precipitation of sphalerite (Mason et al., 2005; Wilkinson et al., 2005, in press; John et al., 2008; Kelley et al., 2009; among others).

The Zn source in the McArthur Basin is mafic volcanic rocks in the early basin fill (Cooke et al., 1998), or alternatively felsic rocks of the basement and siliciclastic rocks in the early basin fill derived by weathering of the felsic basement component (Gigon et al., 2020). Because all these potential sources are expected to have a crustal δ^{66}Zn signature (Fig. 6a), the crustal Zn isotope composition of the McArthur River ores implies that leaching of Zn from the source(s) was either quantitative, resulting in muted Zn isotope fractionation signatures, or was not associated with significant Zn isotope fractionation. The same reasoning holds if mixing of multiple Zn-bearing fluids in formation of the McArthur River deposit occurred (Gigon et al., 2020). This is because each fluid would have inherited a (near-) crustal Zn isotope signature from the sources (mafic igneous rocks or felsic igneous rocks and siliciclastic sedimentary rocks). In the unlikely case of contrasting Zn isotope fingerprints, however, the narrow range of recorded δ^{66}Zn values requires that all the involved fluids and contained metals were homogenized prior to ore formation. The last process to consider is Zn isotope fractionation during fluid evolution. Whereas equilibrium fractionation of Zn isotopes is poorly understood, it has been suggested that the Zn isotope signatures of many major Zn-Pb deposits record influence by kinetic isotope fractionation during sphalerite precipitation, which is a function of Zn disequilibrium in solution; i.e., a high degree of disequilibrium should promote increased kinetic isotope fractionation

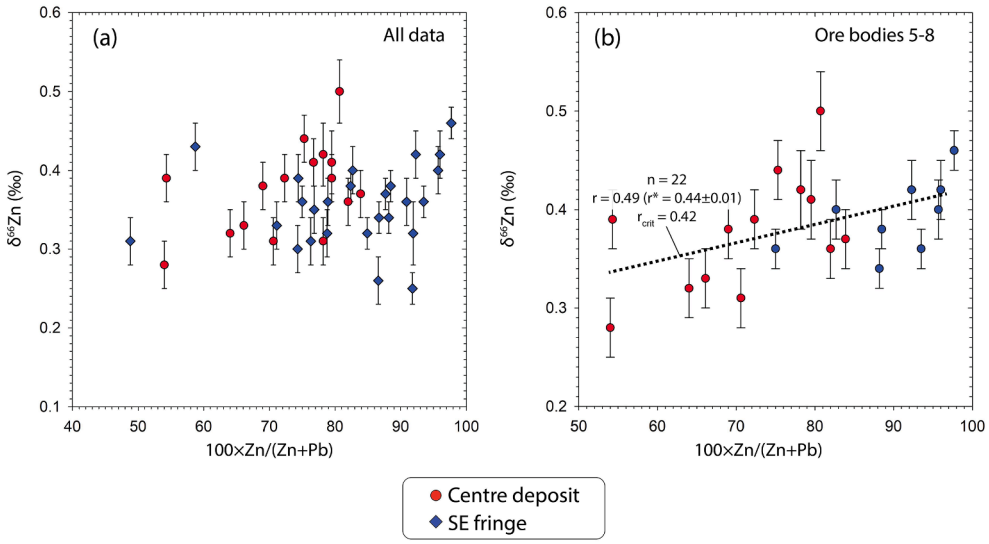

Fig. 8. Plots of 100 × Zn/(Zn + Pb) and δ^{66}Zn in ore samples from the McArthur River Zn-Pb-Ag deposit. Data are shown for samples from (a) all the drill cores, and (b) from ore bodies 5–8. Note the statistically significant correlation (r, $r^* > r_{crit}$) between 100 × Zn/(Zn + Pb) and δ^{66}Zn values in the ore bodies 5–8 (b); n = sample size; r = Pearson correlation coefficient without consideration of the reported errors; r* = Pearson correlation coefficient calculated under consideration of the reported errors (determined by adaption of the Monte Carlo based method described in Curran, 2015); r_{crit} = critical Pearson's r value for a defined sample size. The whole-rock Zn and Pb data are from Spinks et al. (2021).

and the preferred partitioning of light Zn isotopes in sphalerite precipitates (Wilkinson et al., 2005; Mason et al., 2008; Kelley et al., 2008). However, the gross effect of kinetic Zn isotope fractionation also depends on precipitation efficiency; i.e., high degrees of Zn saturation (batch precipitation) would account for a narrow and uniformly distributed Zn isotope composition, and slow sulfide precipitation for a more variable δ^{66}Zn distribution. As supported by the kinetic Zn isotope fractionation model in Fig. 10, the remarkably invariant δ^{66}Zn signature of the analyzed ores is clearly consistent with efficient, (near-) quantitative metal precipitation from Zn-saturated fluids with a crustal Zn isotope composition.

Whereas the McArthur River Zn-Pb-Ag sulfide ores show a relatively homogeneous Zn isotope composition, locally, there appear to be subtle variations between δ^{66}Zn, relative metal abundances [100 × Zn/(Zn + Pb) and Zn/Ag], and deposit stratigraphy. At the centre of the deposit, the δ^{66}Zn, 100 × Zn/(Zn + Pb), and Zn/Ag values of whole rock samples increase with increasing depth, whereas an inverse trend may be prevalent in the south-eastern fringe of the deposit (Figs. 8 and 9). These variations may relate to cooling and evolution of fluid chemistry. Previous studies (e.g., Huston and Large, 1987) demonstrated that the saturation of Zn and Pb in hydrothermal fluids, and hence the ratio between these elements in the ores, may be dictated by the temperature-dependent solubilities of prevailing aqueous Zn- and Pb- (chloride) complexes. Because Pb saturation is attained at higher temperatures than Zn saturation, 100 × Zn/(Zn + Pb) values should increase with decreasing temperature. Silver preferentially partitions into galena relative to sphalerite (e.g., George et al., 2016), causing Zn/Ag ratios to follow 100 × Zn/(Zn + Pb) variations. Hence, the covariations between δ^{66}Zn, 100 × Zn/(Zn + Pb) and Zn/Ag across at least some parts of the McArthur River Zn-Pb-Ag deposit (the shallowest ore bodies 5–8; Fig. 8b) supports the interpretation that the observed Zn isotope variations could relate to closed-system kinetic (Rayleigh-type) isotope fractionation during fluid cooling and sphalerite precipitation (Fig. 10). Nevertheless, the near-quantitative precipitation of Zn led to relatively muted isotopic fractionation and minuscule variation in δ^{66}Zn. Similarly, this (near-) quantitative precipitation of Zn as sphalerite would have muted the effects of any other potential controls on Zn isotopes, such as pH-dependent Zn isotope fractionation between chloride, sulfide, sulfate, and carbonate complexes in the fluid (Fujii et al., 2010, 2011; Bryan et al., 2015).

Although the recorded Zn isotope data of the McArthur River Zn-Pb-Ag ores do not constrain their timing of formation with respect to the host rock, it is important to evaluate the implication of the observed limited range in δ^{66}Zn values for ore formation models. To reiterate, one interpretation places the McArthur River Zn-Pb-Ag deposit into a SEDEX (sedimentary exhalative) formational framework, in which hydrothermal fluids were expelled into the water column from active faults, and base metal sulfides precipitated from basinal metalliferous brines (e.g., Croxford, 1968; Croxford and Jephcott, 1972; Large et al., 1998; Ireland et al., 2004a,b). In contrast, in diagenetic-epigenetic models, the sulfide ores represent sub-seafloor replacement of carbonate within the host rock (e.g., Eldridge et al., 1993; Hinman, 1996; Perkins and Bell, 1998; Logan et al., 2001; Spinks et al., 2021). In syngenetic models, the limited spatial and stratigraphic spread of δ^{66}Zn values implies i) rapid precipitation of sphalerite from a basinal, ground-hugging brine that quickly reached all parts of the sub-basin, and ii) no substantial, temporal Zn isotope evolution between formation of the oldest (stratigraphically lowest) and youngest (stratigraphically highest) ore bodies. In diagenetic-epigenetic mineralization models, the limited range in δ^{66}Zn implies rapid carbonate replacement and fluid reduction (mediated by organic matter), and hence batch precipitation of sphalerite in the subsurface.

5.2. *Zinc isotopes as a tool for mineral exploration?*

Non-traditional stable isotope systems such as Zn have been suggested to be applicable in mineral exploration (e.g., Shanks, 2014; Spinks and Uvarova, 2019; Matt et al., 2020; Wilkinson et al., in press). Zinc isotopes may be particularly useful where earliest-formed ores deposited by relatively high-temperature fluids that show light Zn isotope signatures compared to distal lower temperature fluids or barren host lithologies (Spinks and Uvarova, 2019).

The applicability of Zn isotopes in the exploration for low-temperature, sediment-hosted Zn sulfide deposits, such as the McArthur River Zn-Pb-Ag deposit, can be reviewed within the "mineral systems" framework. This approach is built on the premise that the formation of sizeable mineralization requires a spatial and temporal coincidence of critical, scale-dependent parameters and processes (*source → extraction → transport → concentration*), which may be translated into scale-hierarchical targeting elements and mappable criteria (McCuaig et al., 2010; McCuaig and Hronsky et al., 2014).

The narrow and non-diagnostic variability of Zn isotope signatures in crustal reservoirs (Fig. 6a) indicates that, at least currently, Zn isotopes cannot distinguish between different crustal sources. Similarly, the currently limited understanding if and how non-quantitative extraction of Zn from metal sources influences Zn isotope fractionation limits the applicability of Zn isotopes for this purpose. In other words, it remains unclear to what degree the Zn isotope composition of ore minerals may

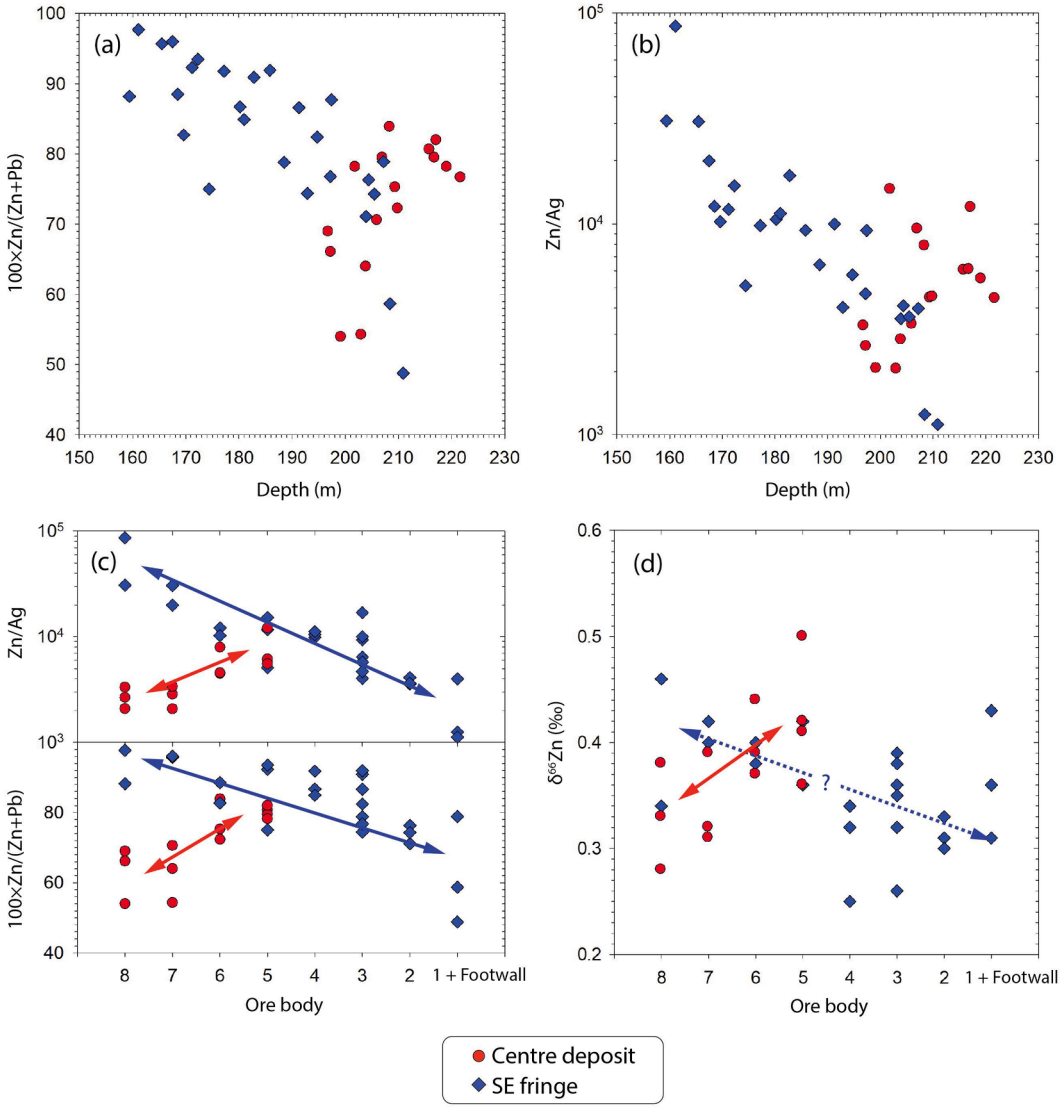

Fig. 9. Covariation of δ^{66}Zn and relative abundances of Zn, Pb and Ag [expressed as 100 × Zn/(Zn + Pb) and Zn/Ag] with depth in drill cores/ore body stratigraphy: a and b) 100 × Zn/(Zn + Pb) and Zn/Ag versus depth in drill cores; c and d) 100 × Zn/(Zn + Pb), Zn/Ag, and δ^{66}Zn in in terms of ore body stratigraphy. Note that (a) and (b) show the results from all analyzed samples (ore bodies + interbeds), whereas (c) and (d) only show data from the ore bodies. In the centre deposit drill core, Zn/Ag, 100 × Zn/(Zn + Pb), and δ^{66}Zn increase with increasing depth (i.e., values increase from ore bodies 7 and 7 to ore bodies 6 and 5, whereas these values appear to decline with increasing depth in the south-eastern fringe drill core. The whole-rock Zn, Pb, and Ag data are from Spinks et al. (2021).

be controlled by isotopic fractionation associated with Zn extraction, and how such an isotopic fractionation signature would compare with Zn isotope variability introduced by fluid mixing processes or equilibrium/kinetic isotope fractionation during fluid evolution (see discussion above and Maréchal and Sheppard, 2002, Wilkinson et al., 2005, Gagnevin et al., 2012, and Veeramani et al., 2015, among others).

Spatial variation in Zn isotope signatures across deposits has been useful in better understanding the transport of metals and tracing fluid flow. For example, Wilkinson et al. (2005) and Gagnevin et al. (2012) reported a systematic spatial variation in δ^{66}Zn values across the Irish sediment-hosted Zn-Pb ore field. This variation was explained by kinetic Zn isotope fractionation during fluid evolution, producing isotopically heavier sphalerite in distal parts of the hydrothermal system, and lighter values proximal to the deposit. This process predicts that Zn isotope compositions could vector towards prospective, relatively high-grade areas (Wilkinson et al., 2005; Gagnevin et al., 2012). The Zn isotope data from the centre and SE fringe of the McArthur River deposit do not show a pronounced pattern, but this could be due to the restricted distance between the two sites (Fig. 3). Further sampling of weakly mineralized lithologies more distal to the main orebodies at McArthur River may be needed to fully test the potential applicability of Zn isotope geochemistry as a vector towards economic-grade mineralisation.

Finally, Zn isotope characterization of ore deposits is useful for approximating the efficiency of metal concentration during ore formation. To reiterate, under conditions of batch sulfide precipitation and efficient Zn concentration, gross effects of Rayleigh-type Zn isotope fractionation should be suppressed, and average Zn isotope compositions of base metal sulfides should approach the source fluids and perhaps even the metal source. Indeed, we interpret the low δ^{66}Zn variability and the lack of a clearly developed Zn isotope fractionation pattern at McArthur River (Figs. 6 and 10) to represent near-quantitative extraction of Zn and/or a lack of isotopic fractionation during Zn extraction in the source, and batch sulfide precipitation during ore formation. Assuming these two processes are required or common for the formation of "giant" Zn deposits, muted isotopic fractionation is expected to be common, and Zn isotopes might thus be of limited use in their exploration.

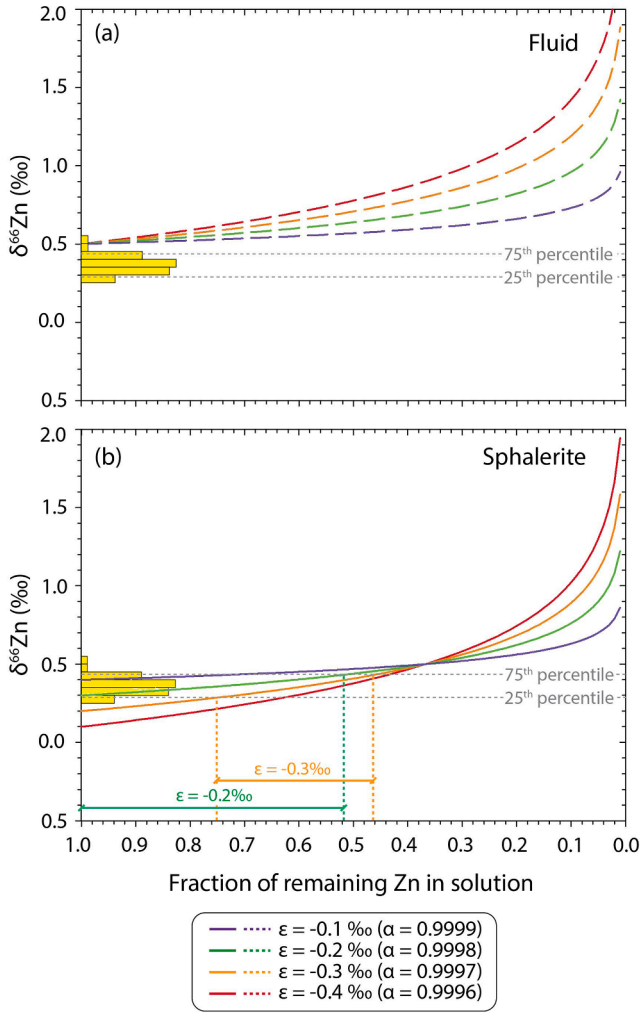

Fig. 10. Kinetic (Rayleigh) fractionation model for Zn isotopes ($\delta^{66}Zn$) in the McArthur River Zn-Pb-Ag deposit. The model tests different sphalerite-fluid Zn isotope fraction factors ($\varepsilon = \delta^{66}Zn_{sphalerite} - \delta^{66}Zn_{fluid}$), assuming a fluid $\delta^{66}Zn$ signature equal to the highest $\delta^{66}Zn$ value in the HYC ores (~0.5 ‰; Table S1). According to this model, and under consideration of reasonable ε values (-0.3 to −0.2; see experimental data in Veeramani et al., 2015), the gross of sulfide ore - that within the 25th and 75th percentile of measured $\delta^{66}Zn$ values - would have precipitated within at least ~ 50 % Zn precipitation from a source fluid, thus indicating efficient metal extraction at the ore deposition site, as consistent with the narrow spread of $\delta^{66}Zn$ values (see discussion in main text, histogram of $\delta^{66}Zn$ values in this figure, and Fig. 6). By comparison, low degrees of precipitation would account for a (highly) skewed distribution in which late stage precipitates would show a shift to increasingly positive $\delta^{66}Zn$ values; i.e., in this model to $\delta^{66}Zn \gg 0.5$ ‰.

6. Conclusions

Our study of the McArthur River Zn-Pb-Ag deposit shows that the sulfide ores exhibit a narrow range of $\delta^{66}Zn$ values (0.25–0.50) that are indistinguishable from the $\delta^{66}Zn$ signature of the continental crust. The recorded small range of Zn isotope compositions are consistent with rapid, (near-) quantitative metal precipitation from a source fluid, and likely indicates (near-) quantitative extraction of Zn from the metal source, or alternatively, a lack of significant isotopic fractionation during non-quantitative Zn leaching. In contrast to previously reported results from the Irish ore field Zn-Ag deposits (Wilkinson et al., 2005), the Red Dog Zn-Pb deposit in Alaska (Kelley et al., 2009), and the Alexandrika volcanic-hosted massive sulphide deposit in Russia (Mason et al., 2005), our results from the centre and periphery of the giant McArthur River Zn-Pb-Ag deposit do not show pronounced Zn isotope fractionation patterns. However, we observe a subtle covariation between $\delta^{66}Zn$ values and abundances of temperature-sensitive base metals (particularly Zn, Pb, and Ag) across some ore bodies of the McArthur River deposit, which supports the proposition that Rayleigh fractionation influences the Zn isotope composition of this type of Zn deposit. Regardless, Zn isotopes would have unlikely been of major importance in discovering the McArthur River deposit, because its crustal $\delta^{66}Zn$ signature does not represent a Zn isotope anomaly, and the lack of strongly developed isotopic fractionation patterns would have hampered the use of Zn isotopes as a geochemical vector for mineral exploration.

Declaration of Competing Interest

The authors declare that they have no known competing financial interests or personal relationships that could have appeared to influence the work reported in this paper.

Acknowledgements

We thank McArthur River Mining Pty Ltd for access to drill core materials and permission to publish the results. The Northern Territory Geological Survey, especially Andrew Wygralak, is thanked for organizing our visit to the mine. Kris Mastermann is thanked for invaluable assistance with access and sampling at McArthur River, and Christopher Hy is thanked for facilitating permission from McArthur River Mining to publish the data. Huayong Chen and Marilena Moroni are thanked for their editorial handling. Ryan Mathur and one anonymous reviewer are thanked for their constructive comments.

Availability of data and material

The datasets generated during and/or analysed during the current study are available from the corresponding author on reasonable request.

Appendix A. Supplementary data

Supplementary data to this article can be found online at https://doi.org/10.1016/j.oregeorev.2021.104545.

References

Bentahila, Y., Ben Othman, D., Luck, J.-M., 2008. Strontium, lead and zinc isotopes in marine cores as tracers of sedimentary provenance: A case study around Taiwan orogen. Chem. Geol. 248 (1-2), 62–82.
Betts, P., Giles, D., 2006. The 1800–1100 Ma tectonic evolution of Australia. Precambr. Res. 144 (1-2), 92–125.
Betts, P.G., Giles, D., Lister, G.S., 2003. Tectonic environment of shale-hosted massive sulfide Pb-Zn-Ag deposits of Proterozoic Northeastern Australia. Econ. Geol. 98, 557–576.
Blaikie, T.N., Kunzmann, M., 2020. Geophyscial interpretation and tectonic synthesis of the Proterozoic southern McArthur Basin, northern Australia. Precambr. Res. 343, 105728.
Brown, M.C., Claxton, C.W., Plumb, K.A., 1978. The Barney Creek Formation and some associated carbonate units of the McArthur Group. Northern Territory. Bureau of Mineral Resources Record 1969/145. p. 59.
Bryan, A.L., Dong, S., Wilkes, E.B., Wasylenki, L.E., 2015. Zinc isotope fractionation during adsorption onto Mn oxyhydroxide at low and high ionic strength. Geochim. Cosmochim. Acta 157, 182–197.
Bull, S.W., 1998. Sedimentology of the Palaeoproterozoic Barney Creek Formation in DDH BMR McArthur 2, southern McArthur Basin, northern Territory. Aust. J. Earth Sci. 45 (1), 21–31.
Chen, H., Savage, P.S., Teng, F.-Z., Helz, R.T., Moynier, F., 2013. Zinc isotope fractionation during magmatic differentiation and the isotopic composition of the bulk Earth. Earth Planet. Sci. Lett. 369-370, 34–42.
Chen, J., Walter, M.R., Logan, G.A., Hinman, M.C., Summons, R.E., 2003. The Paleoproterozoic McArthur River (HYC) Pb/Zn/Ag deposit of northern Australia: Organic geochemistry and ore genesis. Earth Planet. Sci. Lett. 210 (3-4), 467–479.
Conway, T.M., John, S.G., 2014. The biogeochemical cycling of zinc and zinc isotopes in the North Atlantic Ocean. Glob. Biogeochem. Cycles 28 (10), 1111–1128.

Conway, T.M., Rosenberg, A.D., Adkins, J.F., John, S.G., 2013. A new method for precise determination of iron, zinc and cadmium stable isotope ratios in seawater by doublespike mass spectrometry. Anal. Chim. Acta 793, 44–52.
Cooke, D.R., Bull, S.W., Large, R.R., McGoldrick, P.J., 2000. The importance of oxidized brines for the formation of Australian Proterozoic stratiform sediment-hosted Pb-Zn (SEDEX) deposits. Econ. Geol. 95, 1–17.
Craddock, P.R., Rouxel, O.J., Ball, L.A., Bach, W., 2008. Sulfur isotope measurement of sulfate and sulfide by high-resolution MC-ICP-MS. Chem. Geol. 253 (3-4), 102–113.
Croxford, N.J.W., 1968. A mineralogical examination of the McArthur lead-zinc-silver deposit. Proc. Aust. Inst. Min. Metall. 226, 97–108.
Croxford, N.J.W., Jephcott, S., 1972. The McArthur lead-zinc-silver deposit, Northern Territory. Australia. Proc. Aust. Inst. Min. Metall. 243, 1–26.
Curran, P.A., 2015. Monte Carlo error analyses of Spearman's rank test. https://arXiv:1411.3816v2.
Davidson, G.J., Dashlooty, S.A., 1993. The Glyde Sub-basin: a volcaniclastic-bearing pullapart basin coeval with the McArthur River base-metal deposit, Northern Territory. Aust. J. Earth Sci. 40 (6), 527–543.
Dick, J.M., Evans, K.A., Holman, A.I., Leach, D., Grice, K., 2014. Combined sulfur, carbon and redox budget constraints on genetic models for the Here's Your Chance Pb-Zn deposit, Australia. GeoResJ. 3-4, 19–26.
Doucet, L.S., Laurent, O., Mattielli, N., Debouge, W., 2018. Zn isotope heterogeneity in the continental lithosphere: New evidence from Archean granitoids of the northern Kaapvaal craton, South Africa. Chem. Geol. 476, 260–271.
Eldridge, C.S., Williams, N., Walshe, J.L., 1993. Sulfur isotope variability in sediment-hosted massive sulfide deposits as determined using the ion microprobe SHRIMP: II. A study of the H.Y.C. deposit at McArthur River, Northern Territory, Australia. Econ. Geol. 88, 1–26.
Fujii, T., Moynier, F., Pons, M.-L., Albarède, F., 2011. The origin of Zn isotope fractionation in sulfides. Geochim. Cosmochim. Acta 75 (23), 7632–7643.
Fujii, T., Moynier, F., Telouk, P., Abe, M., 2010. Experimental and theoretical investigation of isotope fractionation of zinc between aqua, chloro, and macrocyclic complexes. J. Phys. Chem. A 114 (7), 2543–2552.
Gagnevin, D., Boyce, A.J., Barrie, C.D., Menuge, J.F., Blakeman, R.J., 2012. Zn, Fe and S isotope fractionation in a large hydrothermal system. Geochim. Cosmochim. Acta 88, 183–198.
Gao, Z., Zhu, X., Sun, J., Luo, Z., Bao, C., Tang, C., Ma, J., 2018. Spatial evolution of Zn-Fe-Pb isotopes of sphalerite within a single ore body: A case study from the Dongshengmiao ore deposit, Inner Mongolia, China. Miner. Deposita 53 (1), 55–65.
George, L.L., Cook, N.J., Ciobanu, C.L., 2016. Partitioning of trace elements in co-crystallized sphalerite-galena-chalcopyrite hydrothermal ores. Ore Geol. Rev. 77, 97–116.
Gibson, G.M., Hutton, L.J., Holzschuh, J., 2017. Basin inversion and supercontinent assembly as drivers of sediment-hosted Pb-Zn mineralization in the Mount Isa region, northern Australia. J. Geol. Soc. 174 (4), 773–786.
Gigon, J., Deloule, E., Mercadier, J., Huston, D.L., Richard, A., Annesley, I.R., Wygralak, A.S., Skirrow, R.G., Mernagh, T.P., Masterman, K., 2020. Tracing metal sources for the giant McArthur River Zn-Pb deposit (Australia) using lead isotopes. Geology 48, 478–482.
Giles, D., Betts, P., Lister, G., 2002. Far-field continental backarc setting for the 1.80-1.67 Ga basins of northeastern, Australia. Geology 30 (9), 823–826.
Hinman, M., 1996. Constraints, timing and processes of stratiform base metal mineralization at the HYC Ag-Pb-Zn deposit, McArthur River. In: Baker, T., Rotherham, J.F., Richmond, J.M., Mark, G., Williams, P.J. (Eds.) MIC '96: new developments in metallogenic research: the McArthur, Mt. Isa, Cloncurry Minerals Province, James Cook University of North Queensland, Economic Geology Research Unit 55, 56-59.
Huang, J., Chen, S., Zhang, X.-C., Huang, F., 2018a. Effects of Melt Percolation on Zn Isotope Heterogeneity in the Mantle: Constraints From Peridotite Massifs in Ivrea-Verbano Zone, Italian Alps. J. Geophys. Res. Solid Earth 123 (4), 2706–2722.
Huang, J., Zhang, X.-C., Chen, S., Tang, L., Wörner, G., Yu, H., Huang, F., 2018b. Zinc isotopic systematics of Kamchatka-Aleutian arc magmas controlled by mantle melting. Geochim. Cosmochim. Acta 238, 85–101.
Huston, D.L., Large, R.R., 1987. Genetic and exploration significance of the zinc ratio (100Zn/[Zn+Pb]) in massive sulfide systems. Econ. Geol. 82, 1521–1539.
Ireland, T., Bull, S.W., Large, R.R., 2004a. Mass flow sedimentology within the HYC Zn-Pb-Ag deposit, Northern Territory, Australia: Evidence for syn-sedimentary ore genesis. Miner. Deposita 39 (2), 143–158.
Ireland, T., Large, R.R., McGoldrick, P., Blake, M., 2004b. Spatial Distribution Patterns of Sulfur Isotopes, Nodular Carbonate, and Ore Textures in the McArthur River (HYC) Zn-Pb-Ag Deposit, Northern Territory, Australia. Econ. Geol 99, 1687–1709.
Isson, T.T., Love, G.D., Dupont, C.L., Reinhard, C.T., Zumberge, A.J., Asael, D., Gueguen, B., McCrow, J., Gill, B.C., Owens, J., Rainbird, R.H., Rooney, A.D., Zhao, M.-Y., Stueeken, E.E., Konhauser, K.O., John, S.G., Lyons, T.W., Planavsky, N. J., 2017. Tracking the rise of eukaryotes to ecological dominance with zinc isotopes. Geobiology 16 (4), 341–352.
Jackson, M.J., Muir, M.D., Plumb, K.A., 1987. Geology of the southern McArthur Basin, Northern Territory. Bureau Min. Resour. Aust. Bull. 220, 315.
John, S.G., 2012. Optimizing sample and spike concentrations for isotopic analysis by double-spike ICPMS. J. Anal. At. Spectrom. 27 (12), 2123. https://doi.org/10.1039/c2ja30215b.
John, S.G., Conway, T.M., 2014. A role for scavenging in the marine biogeochemical cycling of zinc and zinc isotopes. Earth and Plan. Sci. Lett. 394, 159–167.
John, S.G., Rouxel, O.J., Craddock, P.R., Engwall, A.M., Boyle, E.A., 2008. Zinc stable isotopes in seafloor hydrothermal vent fluids and chimneys. Earth and Plan. Sci. Lett. 269, 17–28.
John, S.G., Kunzmann, M., Townsend, E.J., Rosenberg, A.D., 2017. Zinc and cadmium stable isotopes in the geological record: A case study from the post-snowball Earth Nuccaleena cap dolostone. Palaeogeogr. Palaeoclimatol. Palaeoecol. 466, 202–208.
Kavner, A., John, S.G., Sass, S., Boyle, E.A., 2008. Redox-driven stable isotope fractionation in transition metals application to Zn electroplating. Geochim. Cosmochim. Acta 72 (7), 1731–1741.
Kelley, K.D., Wilkinson, J.J., Chapman, J.B., Crowther, H.L., Weiss, D.J., 2009. Zinc isotopes in sphalerite from base metal deposits in the red dog district, northern Alaska. Econ. Geol. 104 (6), 767–773.
Kunzmann, M., Halverson, G.P., Sossi, P.A., Raub, T.D., Payne, J.L., Kirby, J., 2013. Zn isotope evidence for immediate resumption of primary productivity after snowball earth. Geology 41, 27–30.
Kunzmann, M., Schmid, S., Blaikie, T.N., Halverson, G.P., 2019. Facies analysis, sequence stratigraphy, and carbon isotope chemostratigraphy of a classic Zn-Pb host succession: The Proterozoic middle McArthur Group, McArthur Basin, Australia. Ore Geol. Rev. 106, 150–175.
Lambert, I.B., 1976. The McArthur lead-zinc-silver deposit: Features in metallogenesis and comparisons with some other stratiform ores. In: Wolfe, K.H. (Ed.), Handbook of stratabound and stratiform ore deposits. Elsevier, Amsterdam, pp. 535–585.
Large, R.R., Bull, S.W., Cooke, D.R., McGoldrick, P.J., 1998. A genetic model for the HYC deposit, Australia, based on regional sedimentology, geochemistry, and sulfide-sediment relationships. Econ. Geol. 93, 1345–1368.
Li, M.-L., Liu, S.-A., Xue, C.-J., Li, D., 2019. Zinc, cadmium and sulfur isotope fractionation in a supergiant MVT deposit with bacteria. Geochim. Cosmochim. Acta 265, 1–18.
Little, S.H., Vance, D., McManus, J., Severmann, S., 2016. Key role of continental margin sediments in the oceanic mass balance of Zn and Zn isotopes. Geology 44 (3), 207–210.
Little, S.H., Vance, D., Walker-Brown, C., Landing, W.M., 2014. The oceanic mass balance of copper and zinc isotopes, investigated by analysis of their inputs, and outputs to ferromanganese oxide sediments. Geochim. Cosmochim. Acta 125, 673–693.
Logan, G.A., Hinman, M.C., Walter, M.R., Summons, R.E., 2001. Biogeochemistry of the 1640 Ma McArthur River (HYC) lead-zinc ore and host sediments, Northern Territory, Australia. Geochim. Cosmochim. Acta 65 (14), 2317–2336.
Logan, R.G., Murray, W.J., Williams, N., 1990. HYC silver-lead-zinc deposit, McArthur River. In: Hughes FF (Ed.), Geology of the Mineral Deposits of Australia and Papua New Guinea. Austral. Inst. Min. Metall. 1, 907-911.
Maréchal, C.N., Nicolas, E., Douchet, C., Albarède, F., 2000. Abundance of zinc isotopes as a marine biogeochemical tracer. Geochem. Geophys. Geosyst. 1, 1999GC000029.
Maréchal, C., Albarède, F., 2002. Ion-exchange fractionation of copper and zinc isotopes. Geochim. Cosmochim. Acta 66 (9), 1499–1509.
Maréchal, C.N., Télouk, P., Albarède, F., 1999. Precise analysis of copper and zinc isotopic compositions by plasma-source mass spectrometry. Chem. Geol. 156 (1-4), 251–273.
Mason, T.F.D., Weiss, D.J., Chapman, J.B., Wilkinson, J.J., Tessalina, S.G., Spiro, B., Horstwood, M.S.A., Spratt, J., Coles, B.J., 2005. Zn and Cu isotopic variability in the Alexandrinka volcanic-hosted massive sulfide (VHMS) ore deposit, Urals. Russia. Chem. Geol. 221, 170–187.
Matt, P., Powell, W., Mathur, R., deLorraine, W.F., 2020. Zn-isotopic evidence for fluid-assisted ore remobilization at the Balmat Zinc Mine, NY. Ore Geol. Rev. 116, 103227. https://doi.org/10.1016/j.oregeorev.2019.103227.
McCuaig, T.C., Beresford, S., Hronsky, J., 2010. Translating the mineral systems approach into an effective exploration targeting system. Ore Geol. Rev. 38 (3), 128–138.
McCuaig, T.C., Hronsky, J.M.A., 2014. The mineral system concept: The key to exploration targeting. Appl. Earth Sci. IMM Trans. Sect. B 18, 153–175.
McGoldrick, P.J., Winefield, P., Bull, S.W., Selley, D., Scott, R., 2010. Sequences, synsedimentary structures, and sub-basins: the where and when of SEDEX zinc systems in the Southern McArthur Basin, Australia. Soc. Econ. Geol. Spec. Publ. 15, 367–389.
Moynier, F., Vance, D., Fujii, T., Savage, P., 2017. The isotope geochemistry of zinc and copper. Rev. Mineral. Geochem. 82 (1), 543–600.
Perkins, W.G., Bell, T.H., 1998. Stratiform replacement lead-zinc deposits: A comparison between Mount Isa, Hilton, and McArthur River. Econ. Geol. 93, 1190–1212.
Pichat, S., Douchet, C., Albarède, F., 2003. Zinc isotope variations in deep-sea carbonates from the eastern equatorial Pacific over the last 175 ka. Earth Planet. Sci. Lett. 210 (1-2), 167–178.
Rawlings, D.J., 1999. Stratigraphic resolution of a multiphase intracratonic basin system: the McArthur Basin, northern Australia. Aust. J. Earth Sci. 46 (5), 703–723.
Revels, B.N., Ohnemus, D.C., Lam, P.J., Conway, T.M., John, S.G., 2014. The isotope signature and distribution of particulate iron in the North Atlantic Ocean. Deep-Sea Res. II Top Stud. Oceanogr. 116, 321–331.
Scott, D.L., Rawlings, D.J., Page, R.W., Tarlowski, C.Z., Idnurm, M., Jackson, M.J., Southgate, P.N., 2000. Basement framework and geodynamic evolution of the Palaeoproterozoic superbasins of north-central Australia: an integrated review of geochemical, geochronological and geophysical data. Aust. J. Earth Sci. 47 (3), 341–380.
Selway, K., Hand, M., Heinson, G.S., Payne, J.L., 2009. Magnetotelluric constraints on subduction polarity reversal: reversing reconstruction models for Proterozoic Australia. Geology 37, 799–802.
Shanks III, W.C., 2014. Stable isotope geochemistry of mineral deposits. In: Scott, S.D. (Ed.) Geochemistry of Mineral Deposits. Treat. Geochem., pp. 59-85.
Siebert, C., Nägler, T.F., Kramers, J.D., 2001. Determination of molybdenum isotope fractionation by double-spike multicollector inductively coupled plasma mass spectrometry. Geochem. Geophys. Geosyst. 2 (7), n/a–n/a.

Sossi, P.A., Nebel, O., O'Neill, H.S.C., Moynier, F., 2018. Zinc isotope composition of the Earth and its behaviour during planetary accretion. Chem. Geol. 477, 73–84.
Spinks, S., Pearce, M., Liu, W., Kunzmann, M., Ryan, C., Moorhead, G., Kirkham, R., Blaikie, T., Sheldon, H., Schaubs, P., Rickard, W., 2021. Carbonate replacement as the principal ore formation process in the Proterozoic McArthur River (HYC) sediment-hosted Zn-Pb deposit, Australia. Econ. Geol. 116, 693–718.
Spinks, S.C., Uvarova, Y., 2019. Fractionation of Zn isotopes in terrestrial ferromanganese crusts and implications for tracing isotopically heterogeneous metal sources. Chem. Geol. 119314.
Telus, M., Dauphas, N., Moynier, F., Tissot, F.L.H., Teng, F.-Z., Nabelek, P.I., Craddock, P. R., Groat, L.A., 2012. Iron, zinc, magnesium and uranium isotopic fractionation during continental crust differentiation: the tale from migmatites, granitoids, and pegmatites. Geochim. Cosmochim. Acta 97, 247–265.
Vance, D., Little, S.H., Archer, C., Cameron, V., Andersen, M.B., Rijkenberg, M.J.A., Lyons, T.W., 2016. The oceanic budgets of nickel and zinc isotopes: the importance of sulfidic environments as illustrated by the Black Sea. Phil. Trans. R. Soc. A 374 (2081), 20150294. https://doi.org/10.1098/rsta.2015.0294.
Veeramani, H., Eagling, J., Jamieson-Hanes, J.H., Kong, L., Ptacek, C.J., Blowes, D.W., 2015. Zinc isotope fractionation as an indicator of geochemical attenuation processes. Environ. Sci. Technol. Lett. 2 (11), 314–319.
Wang, D.a., Zheng, Y., Mathur, R., Wu, S., 2018. The Fe-Zn Isotopic Characteristics and Fractionation Models: Implications for the Genesis of the Zhaxikang Sb-Pb-Zn-Ag Deposit in Southern Tibet. Geofluids 2018, 1–23.
Wang, Z.-Z., Liu, S.-A., Liu, J., Huang, J., Xiao, Y., Chu, Z.-Y., Zhao, X.-M., Tang, L., 2017. Zinc isotope fractionation during mantle melting and constraints on the Zn isotope composition of Earth's upper mantle. Geochim. Cosmochim. Acta 198, 151–167.
Wilkinson, J.J. (in press) The potential of Zn isotopes in the science and exploration of ore deposits.
Wilkinson, J.J., Weiss, D.J., Mason, T.F.D., Coles, B.J., 2005. Zinc isotope variation in hydrothermal systems: Preliminary evidence from the Irish midlands ore field. Econ. Geol. 100, 583–590.
Williams, N., 1978. Studies of the base metal sulfide deposits at McArthur River, Northern Territory, Australia: II. The sulfide-S and organic-C relationships of the concordant deposits and their significance. Econ. Geol. 73, 1036–1056.
Xu, L.-J., Liu, S.-A., Wang, Z.-Z., Liu, C., Li, S., 2019. Zinc isotopic compositions of migmatites and granitoids from the Dabie Orogen, central China: Implications for zinc isotopic fractionation during differentiation of the continental crust. Lithos 324-325, 454–465.
Zhou, J.-X., Huang, Z.-L., Lv, Z.-C., Zhu, X.-K., Gao, J.-G., Mirnejad, H., 2014a. Geology, isotope geochemistry and ore genesis of the Shanshulin carbonate-hosted Pb-Zn deposit, southwest China. Ore Geol. Rev. 63, 209–225.
Zhou, J.-X., Huang, Z.-L., Zhou, M.-F., Zhu, X.-K., Muchez, P., 2014b. Zinc, sulfur and lead isotopic variations in carbonate-hosted Pb-Zn sulfide deposits, southwest China. Ore Geol. Rev. 58, 41–54.